ASTRO-H

INSTRUMENT CALIBRATION REPORT
Mirror Definition File
ASTH-HXT-CALDB-MIRROR

Version 0.2

December 22, 2016

JAXA / GSFC

Prepared by: A. Furuzawa, H. Awaki, S. Yamauchi, H. Matsumoto, I. Mitsuishi et al., GSFC *Hitomi* Data Science Center

Table of Contents

CHANGE RECORD PAGE (1 of 1)

DOCUMENT TITLE : Mirror Definition File			
ISSUE	DATE	PAGES AFFECTED	DESCRIPTION
Version 0.1	10 Mar 2016	All	First Release
Version 0.2	22 Dec 2016	All	Second Release

1 Introduction

1.1 Purpose

This document describes the elements and structure of the HXTs related to the telescope performance, implementation of them to the raytracing code (xrtraytrace) and how to create the CALDB files used by xrtraytrace.
The CALDB file structure is define in the ASTH-SCT-04 and available from the CALDB web page at http:// hitomi.gsfc.nasa.gov.

1.2 Scientific Impact

As shown in Fig. 1, the HXT consists of the primary and secondary parts and each part is divided into 3 segments containing 213 reflector shells confocally nested. Each of top and bottom edges of reflectors in a segment are positioned by 8 alignment bars arranged radially. A fan-shaped region sectioned by neighboring alignment bars is defined as 'sector'. The radial position of alignment bars were tuned to focus X-rays as narrowly as possible. Each reflector has figure errors in both radial and circumferencial directions. Those figure errors of reflectors and remaining misalignments cause a scattering and blurring images focused by each of local parts of aperture of the telescope.

Because the reflectivity strongly depends on the incident angle, we divided the reflectors into 14 groups by their incident angles, and optimized the multilayer design for each group. The reflectivity of the multilayer depend on the multilayer design and interfacial roughness.

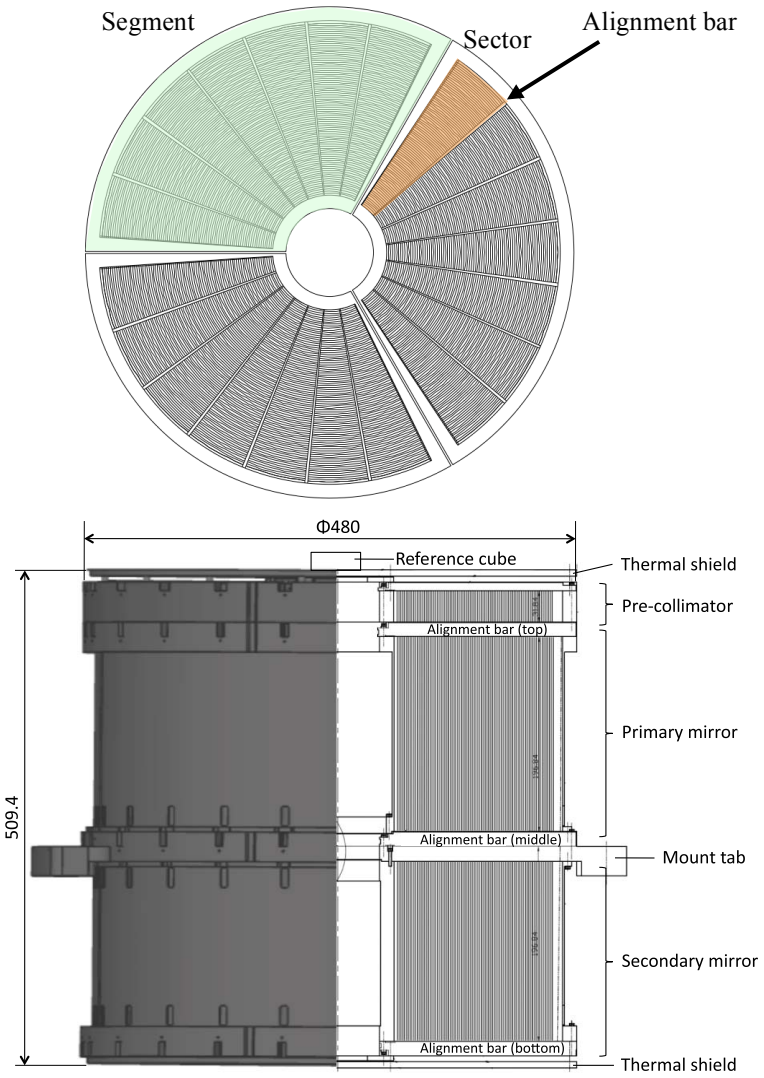

Fig. 1 Structure of the HXT

Thus the telescope performance such as an effective area, a vignetting function, a Point Spread Function (PSF) and an Encircled Energy Function (EEF) strongly depends on those local properties of reflectors.

In the raytracing code (xrtraytrace), each reflector is defined as a series of subfoils arranged in a circumference direction, and each subfoil has a different position, orientation, reflection profile and multilayer structure as local properties. The implementation of subfoils and their properties enable us to estimate actual performance of the telescope.

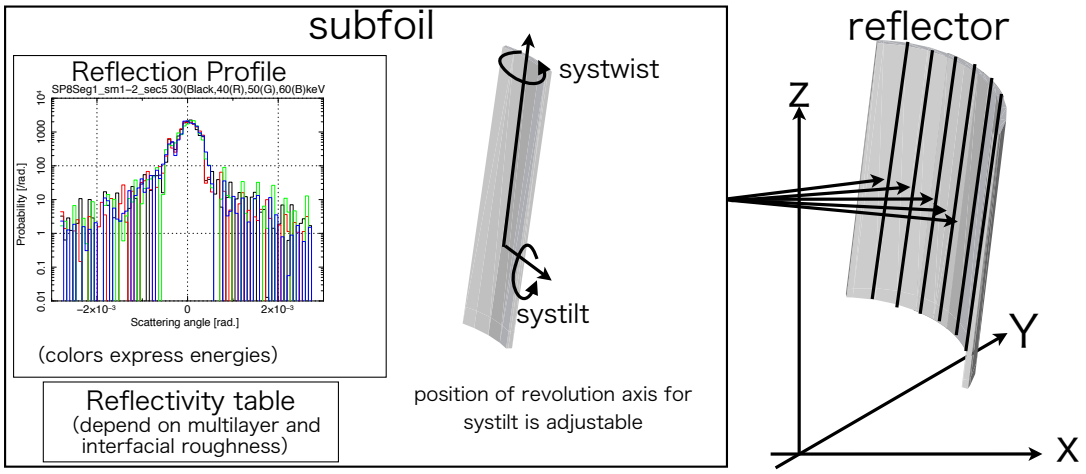

Fig. 2 implementation of subfoil

The CALDB files are used to implement local properties derived from the measurements to reproduce the effective area and the PSF of the HXTs.

Contents of CALDB files

1) Mirror file
The mirror file contains following 6 extensions.

i) MIRROR extension : definitions of subfoils and their parameters for reflectors
A subfoil is defined as a 'sector' part of a reflector defined by alignment bars. The definition of subfoil unit is commonly used for a primary reflector, a secondary reflector and a precollimetor blade.
Following parameters are defined for each subfoil.

- Positions of edge points in cylindrical coordinate
  Design values are stored.

- Names of reflectivity tables for the front side and back side of reflectors
  A reflectivity table for a front side is calculated for each multilayer group. For a back side, it is defined to refer the common reflectivity table.

- Name of the reflection profile table for the front side of reflectors
  Aperture is divided into regions defined with the boundaries of multilayer groups and sector boundaries (the alignment bars), and the common reflection profile is defined for primary and secondary subfoils in each region.

- Misalignment in the direction of tilt and twist
  In the current version, they were derived from flux weighted mean of centroids of spot images (see 2.2).
  They may be tuned according to in-flight EEF (PSF) calibration.

ii) OBSTRUCT extension : definitions of support structures obstructing a photon
Support structure such as alignment bars and sector covers are implemented as a plane blocking photons. The plane is defined by X-Y coordinates of its vertexes and plane's Z coordinate. Therefore, the plane is parallel to an X-Y plane.
Design values are stored.

iii) SEGMENT extension : definitions of misalignment of each segment
Displacement and orientation of each segment from the design value are defined.
In the current version, design values are stored (displacement and orientation = 0).
They may be tuned according to in-flight effective area, vignetting and EEF (PSF) calibration.

iv) COLLIMATOR extension : definitions of subfoils and their parameters for precollimator blades
Definition of subfoil is the same as that of a reflector. For both front side and back side, the same reflectivity table and reflection profile are defined to be referred as those for back side of reflectors.
They may be tuned according to in-flight effective area, vignetting and EEF (PSF) calibration.

v) SURFACE extension : definitions of multilayer structure and its interfacial roughness
Design values of multilayer structures are stored.
Roughness parameters are derived to fit the energy dependence of the effective area of each multilayer group according to the ground calibration data.
Roughness may be tuned according to in-flight effective area calibration.

vi) AZIMUTHALSTRUCT extension : definitions of thermal shield geometry and materials
Design values are stored.

2) Scatter file: reflection profiles for front side and back side of reflectors and precollimator blades
Front side reflection profiles were determine by on-ground measurement data (see 2.2).
They may be tuned according to in-flight effective area, vignetting and EEF (PSF) calibration.

.

For precollimator blades, a common reflection profile is used for both front and back side. In the current version, below 12 keV, the profiles are the same as those applied for back side reflection of the Suzaku XRT reflectors. Above 12 keV, the profile at 12 keV is applied.
The reflection profile for precollimator blades and back side of reflectors will be updated after finishing analysis of the on-ground measurement in future.

3) Reftrans file
It contains reflectivity and transmissivity tables for all multilayer groups calculated by xrtreftable with the current CALDB files, reflectivity tables for back side of reflectors and both side of precollimator blades, and mass absorption coefficient table for the thermal shield and the central cover.

For reflection at back side of reflectors and precollimator blades, a common reflectivity table is used. The current version includes the reflectivity table measured with Suzaku XRT reflectors below 20 keV and calculated table assuming aluminum smooth surface above 20 keV.
The reflectivity tables for precollimator blades and back side of reflectors will be updated after finishing analysis of the on-ground measurement in future.

4) atomicScattering file
AtomicScattering file provides various tables of atomic scattering factor (f1 and f2) from different literatures.
Simulation results in this document and deriving optimum interfacial roughness were obtained with atomic scattering factors in the extension 'HenkeSskChant' in the current atomicScattering file. The scattering factor in 'HenkeSskChant' come from S.Sasaki 1989 (KEK Report, 88-14, 1-136) and S.Sasaki 1990 (KEK Report, 90-16, 1-143) at energies above 4275.34 eV, and Henke 1993 (Atomic Data and Nuclear Data Tables Vol. 54 (no.2), 181-342) at energies less than and equal to 4275.34 eV.
They may be tuned with in-flight data, if it is nessesary.

2 Release CALDB 20160310

Filename	Valid data	Release data	CALDB Vrs	Comments
ah_hx1_mirror_20140101v001.fits	2014-01-01	2016-03-10	001	Mirror
ah_hx2_mirror_20140101v001.fits	2014-01-01	2016-03-10	001	Mirror
ah_hx1_scatter_20140101v001.fits	2014-01-01	2016-03-10	001	Scatter
ah_hx2_scatter_20140101v001.fits	2014-01-01	2016-03-10	001	Scatter
ah_hx1_reftrans_20140101v001.fits	2014-01-01	2016-03-10	001	Reftrans
ah_hx2_reftrans_20140101v001.fits	2014-01-01	2016-03-10	001	Reftrans
ah_gen_atmsca_20140101v001.fits	2014-01-01	2016-03-10	001	atomicScatter

2.1 Data Description

Ground calibration data used for deriving parameters stored in CALDB files have been taken at the SPring-8 BL-20B2 in Nov. 2012 for HXT-1 and Oct. 2013 for HXT-2. Details of the ground calibration are described in Awaki et al. 2014 (Applied Opics, 53, 32, 7664).

An X-ray beam was collimated into 10 mm x 10 mm rectangular shape and one segment of the HXT was fully covered by a mosaic mapping method (spot scan measurement) with that X-ray beam. Each X-ray beam forms a image (local spot image) which has different centroid and a profile on the focal plane (Fig. 3). It is due to figure error and misalignment of subfoils.

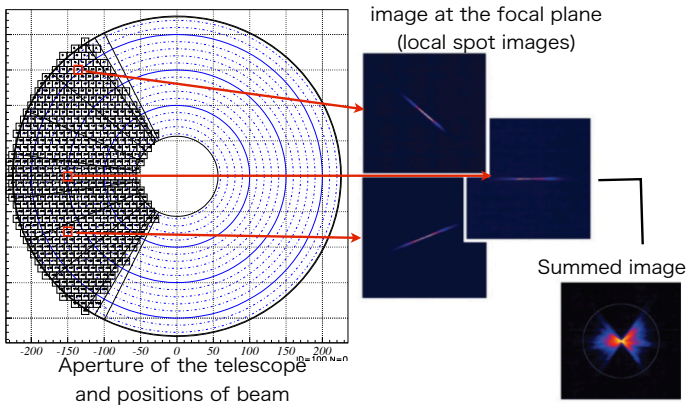

Fig. 3 Spot scan measurement

As described in 2.2, an offset from an ideal focus point was converted into the misalignment parameters, systilt and systwist. Reflection profiles for fromt side of subfoils were also derived from the one dimensional profiles of local spot images. Measurements with the mosaic exposure method have been done at 20 (HXT1 only), 30, 40, 60 and 70 keV.

For assessment of atomic scattering factors of Pt and C around Pt L and K absorption edges, reflectivity of Pt/C multilayers has been measured at SPring-8 BL-01B in 2014 (Fig. 4).

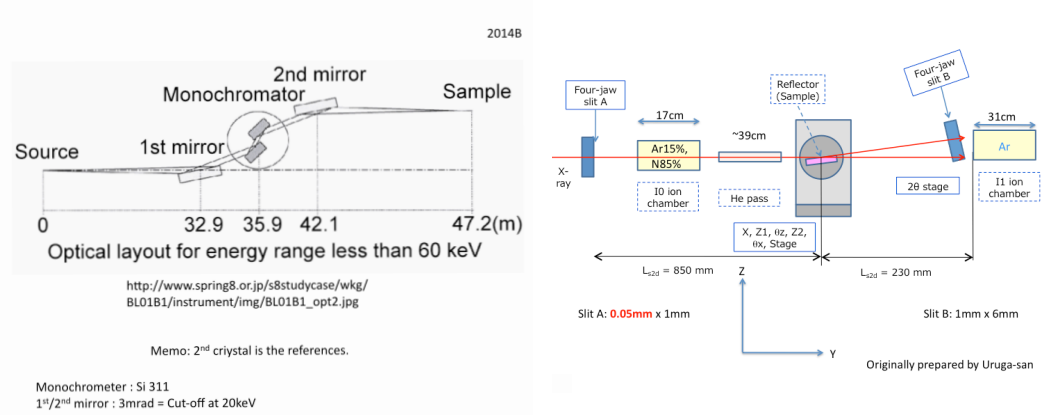

Fig. 4 Reflectivity measurement at SPring-8 BL-01B
Configuration of BL-01B (left) and instrument and sample setup (right)

2.2 Data Analysis

systilt and systwist

Fig. 5 shows schematic view to derive systilt and systwist parameters of a subfoil in the mirror file from the spot images. The systilt and systwist parameters were derived from a centroid of each spot image measured at 30 keV because the profile at 30 keV has smallest statistical and systematic uncertainty even for the outer most spot.

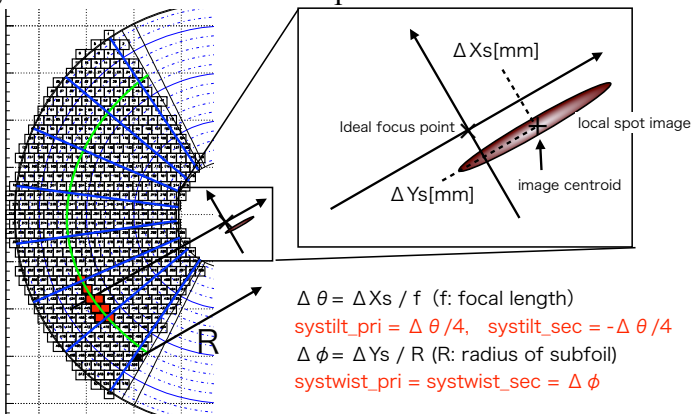

Fig. 5 Schematic view of the measurement data and determination of misalignment parameters; systilt and systwist.

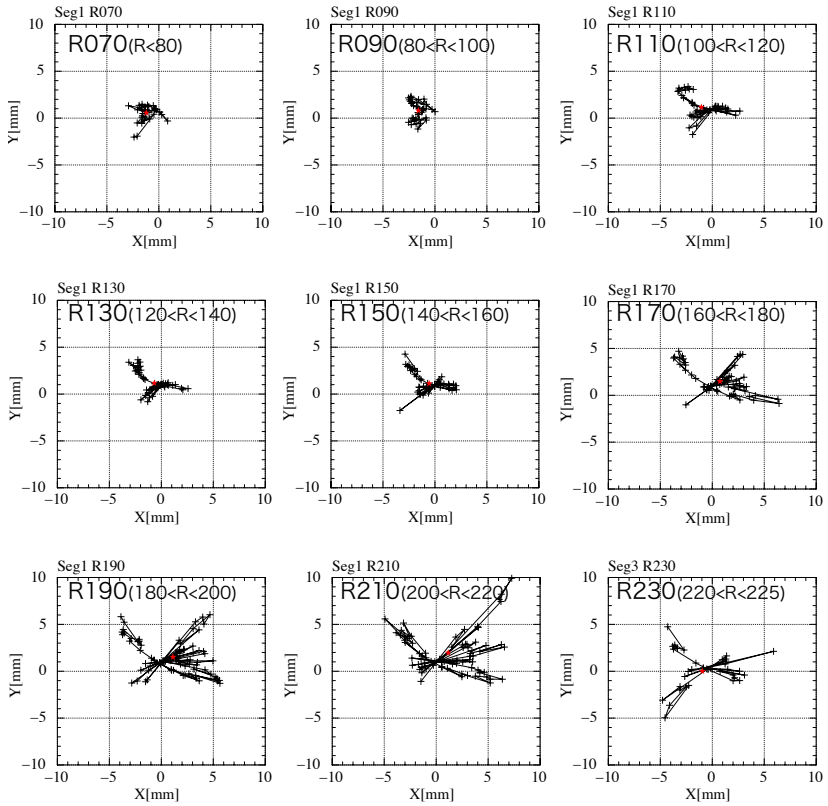

Fig. 6 distribution of centroids of local spot images in each annulus of aperture for HXT2 Black and red crosses represent positions of centroids of local spot images and weighted mean of them, respectively

Scattering Profile for front side of reflectors

Aperture is divided into regions defined with the boundaries of multilayer group and sector boundaries, and averaged 1-dimensional profiles of the local spot images corresponding to those regions were derived. Front side reflection profiles of sub-foils of reflectors were obtained by deconvolution using FFT from those 1-dimentional profile with an assumption that primary and secondary reflectors have the same reflection profile.

Fig. 7 shows a profile of a spot image and derived single-reflection profile by deconvolution In the current scattering file, the reflection profiles at 30, 40, 50 and 60 keV are implemented. For HXT2, profiles widened by a factor of 1.12 are used to adjust an encircled energy function of the HXT2 to the measured one. For HXT1, adjustment of encircled energy function has not been done.

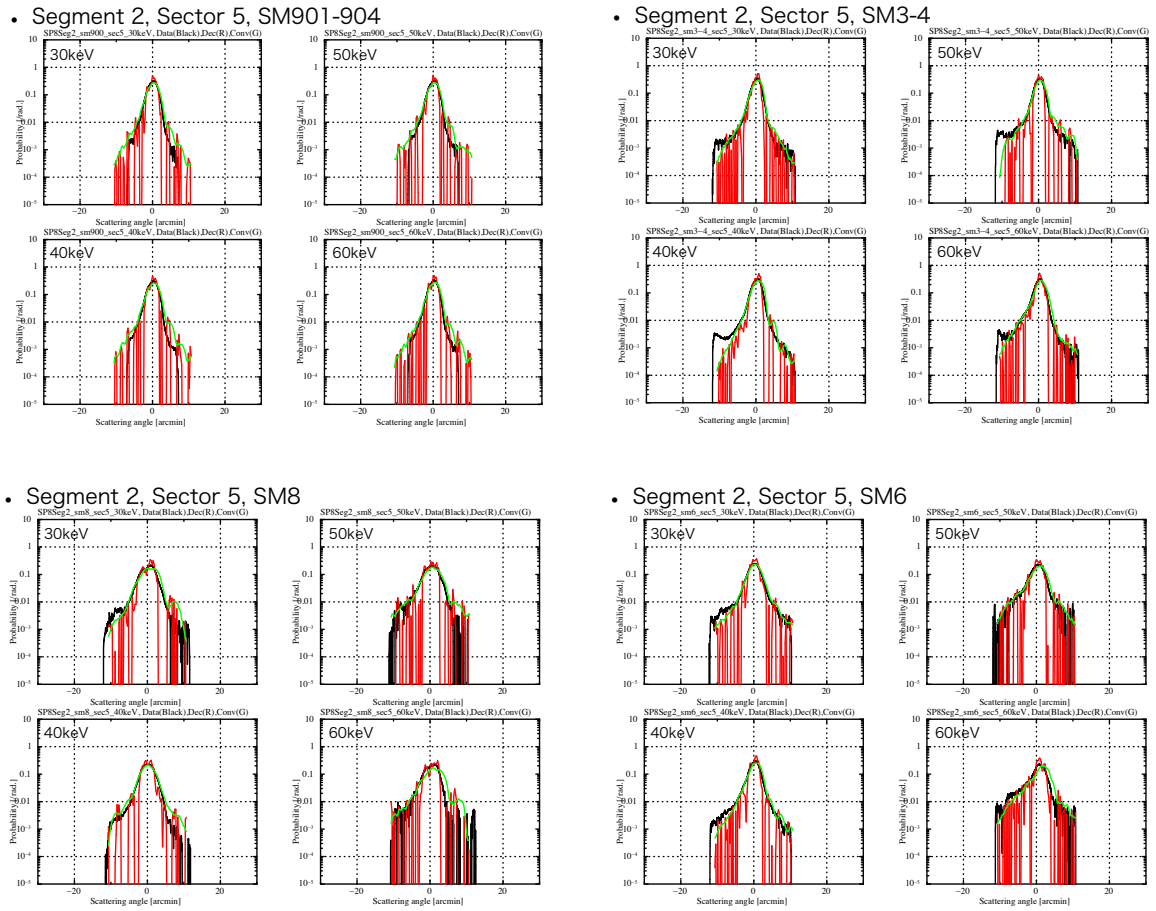

Fig. 7 1-dimensional profiles for HXT2. Black : local spot image, Red : deconvolved reflection profile, Green: convolved profile derived from the reflection profile.

Reflectivity Curve

The measurement reflectivity of Pt/C multilayer mirror at energies around Pt-L and Pt-K absorption edges is consistent with the reflectivity calculated from the scattering factors of 'HenkeSskChant' for interesting range of incident angle and energies of absorption edge (Fig. 8).

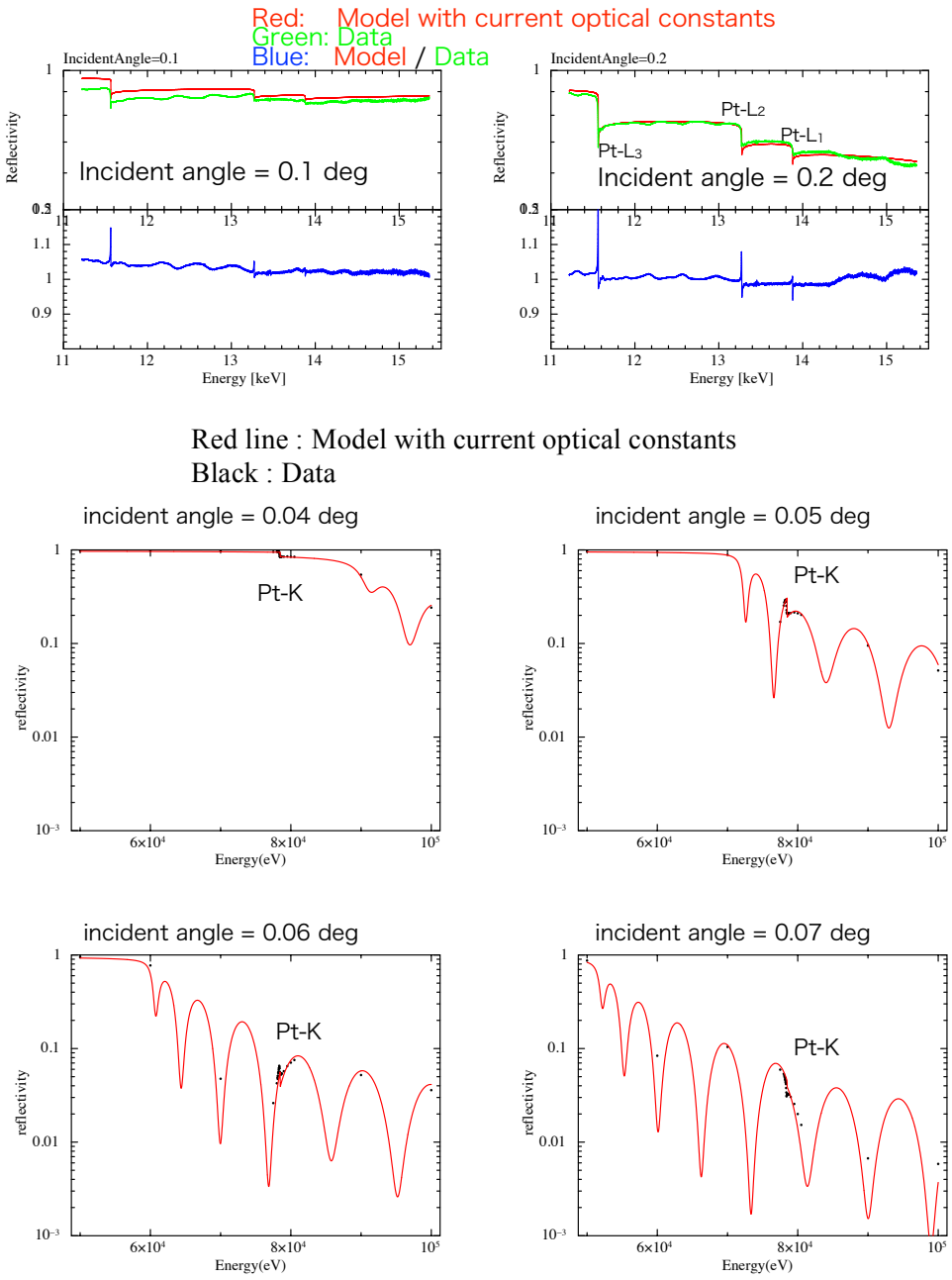

Fig. 8 Reflectivity of Pt/C multilayer. Top two figures show the reflectivity at energies around Pt-L edges at incident angles of 0.1 and 0.2 degrees; red: model with current optical constants, green: measured data, blue: ratio of model to data.
Reflectivity including Pt-K edge at incident angles of 0.04, 0.05, 0.06 and 0.07 degrees are shown in bottom 4 figures; red line: model with current optical constants, black dots: measured data

2.3 Results

Summary of the current settings in the CALDB files

1) Mirror file

   i) MIRROR extension
      - Positions of edge points in cylindrical coordinate
        Design values
      - Misalignment in the direction of tilt and twist
        Determined from ground calibration data.

   ii) OBSTRUCT extension
        Design values

   iii) SEGMENT extension
        Design values

   iv) COLLIMATOR extension
        Design values

   v) SURFACE extension
        Design values of multilayer structures
        Roughness derived to fit the energy dependence of the effective area of each multilayer group obtained by the ground calibration.

   vi) AZIMUTHALSTRUCT extension : definitions of thermal shield geometry and materials
        Design values

2) Scatter file : reflection profiles for front side and back side of reflectors and precollimator blades
   Front side of reflectors : derived from spot image profile obtained by ground calibration
   Back side of reflectors, precollimator blades : profile of back side of Suzaku XRT reflector

3) Reftrans file
   Front side of reflectors : calculated by xrtreftable with the current CALDB files
   Back side of reflectors, precollimator blades : reflectivity tables for back side of reflectors and both side of precollimator blades from Suzaku data blow 20 keV and calculation above 20 keV, and mass absorption coefficient table for the thermal shield and the central cover from calculation with the current absorption coefficients.

4) atomicScattering file
   'HenkeSskChant' is used for calibration

On-axis Effective Area and HPD

Fig. 9 and Fig. 10 show on-axis effective area and HPD estimated by xrtraytrace with the current CALDB files in comparison to the values obtained on the ground for HXT1 and HXT2,

respectively. Effective area was derived by accumulating flux within a radius of 4.3' (16 mm at the focal plane).
Discrepancy between the simulated and the measured effective area is smaller than +9/-7 % at energies of 8, 20, 30, 40, 50, 60 and70 keV.

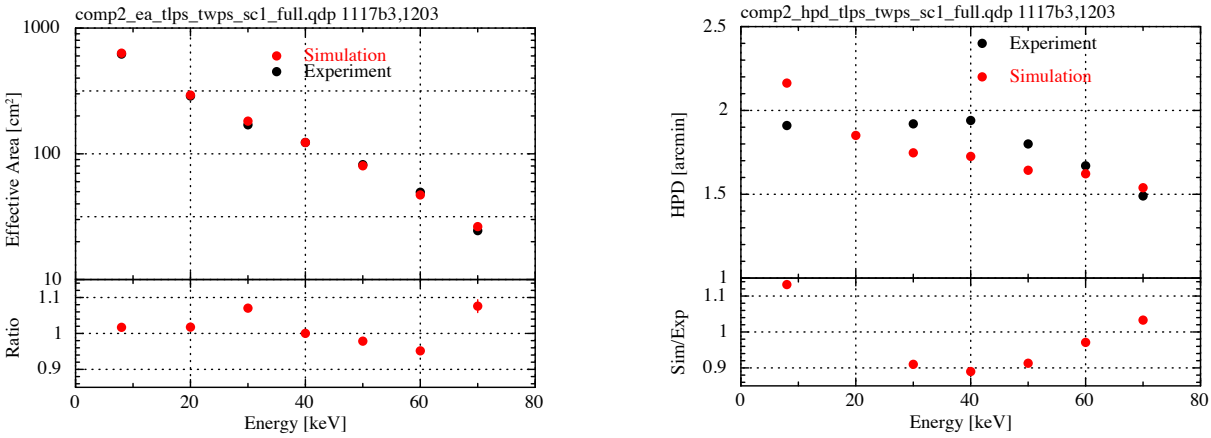

Fig. 9 Effective area (left) and HPD (right) of the HXT-1 (full telecope without the thermal shields)

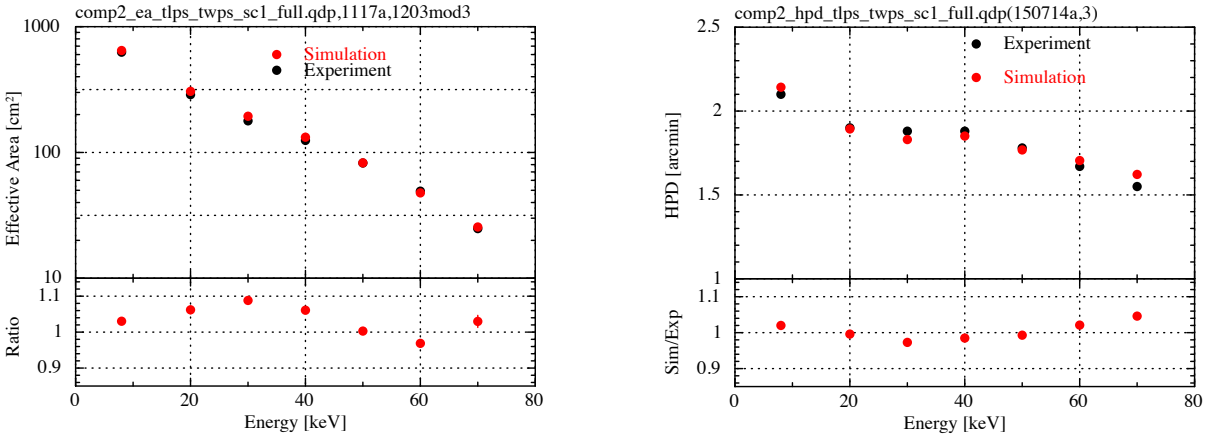

Fig. 10 Effective Area (left) and HPD (right) of the HXT-2 (full telescope without the thermal shields)

On-axis EEF and PSF

Fig. 11 and Fig. 12 show EEF and PSF of HXT1 and HXT2, respectively. EEF and PSF were calculated from a image normalized so that a flux within a radius of 6.24' is equal 1 for both of

simulated and measured data, and PSF is azimuthally averaged. The simulated EEF is in good agreement with the measured one EEFs as the difference is smaller than 5 % at a radius larger than 2 arcmin. For PSF, discrepancy is less than 20 % within a radius of 4 arcmin. At a radius > 4 arcmin, simulated PSF is 20 - 40 % fainter than the measured one.

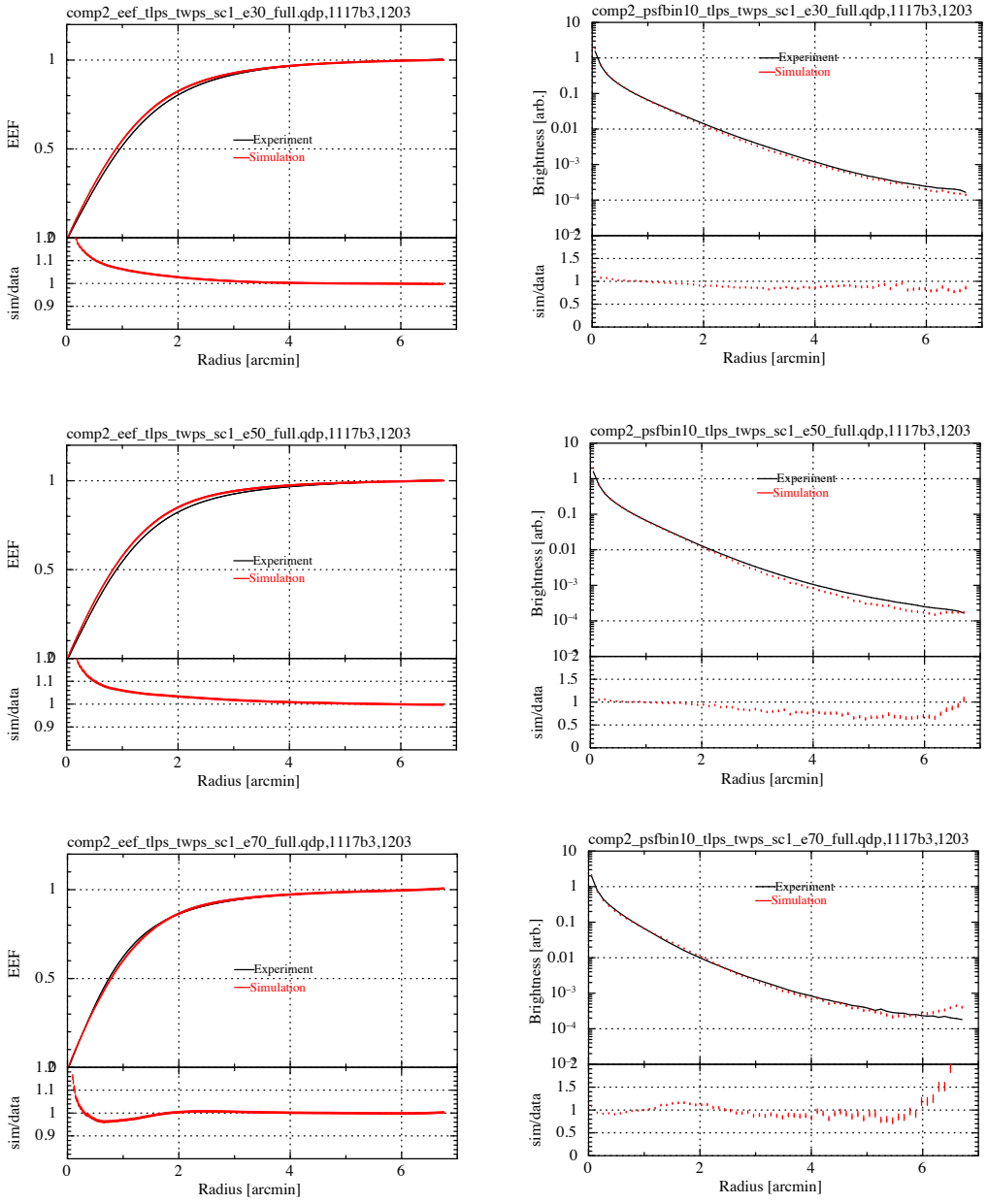

Fig. 11 EEF (left) and PSF (right) of HXT-1 at 30 keV (top), 50 keV (middle), 70 keV (bottom)

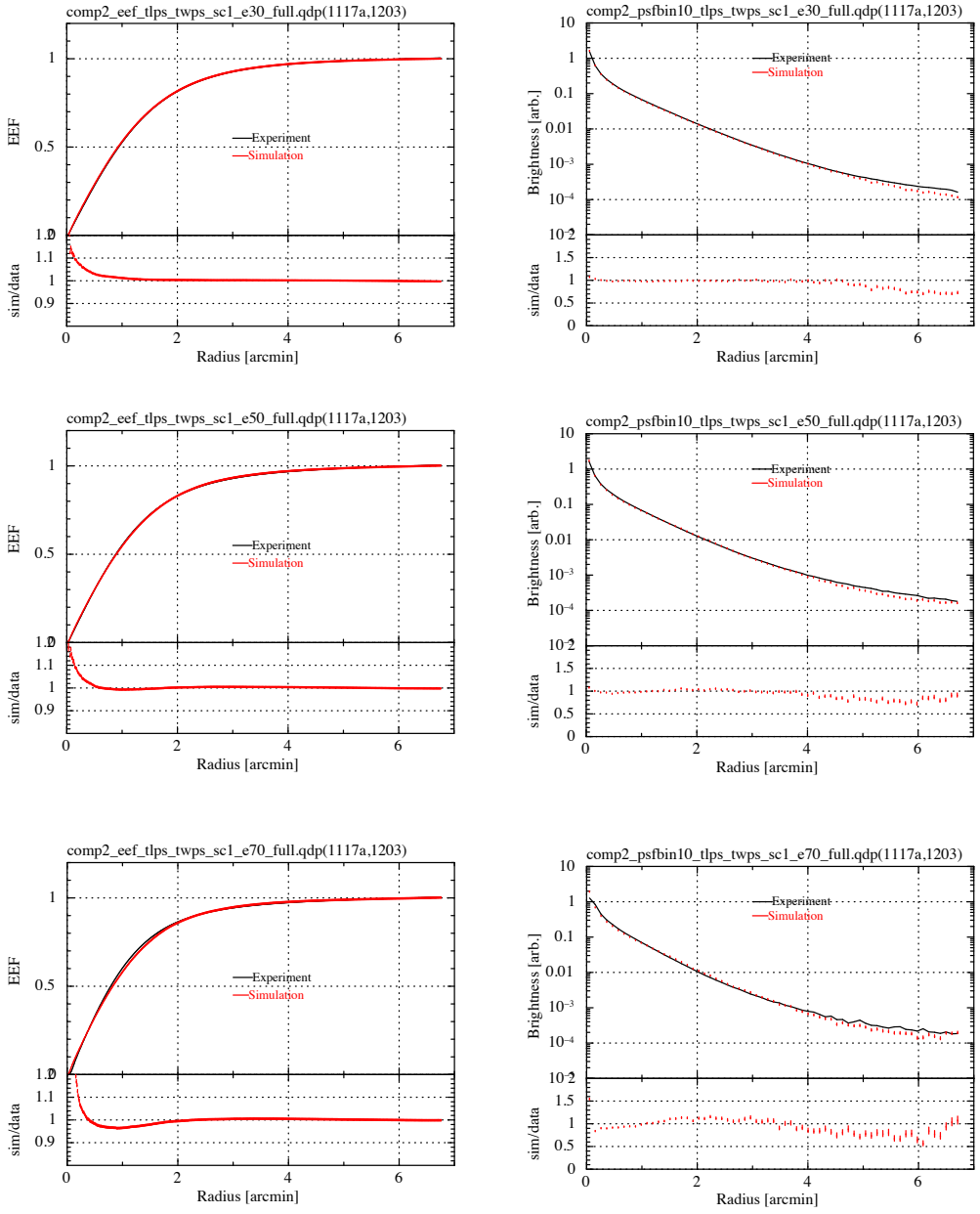

Fig. 12 EEF (left) and PSF (right) of HXT-2 at 30 keV (top), 50 keV (middle), 70 keV (bottom)

The Crab pulsar EEF

The Encircled Energy Function (EEF) was also measured from inflight *Hitomi* data. For the Crab pulsar image in 5-80 keV band the EEF was generated by excluding a contribution from an extended emission region from the Crab nebula by subtracting an image extracted in the off-pulse phase and normalized with the dead-time corrected exposure time.

Fig. 12(b) shows the systematic difference between the observed and simulated EEF. As shown in Fig. 12(b), while the simulated EEF agrees well with the EEF measured on the ground, the

Crab EEF is systematically larger than the simulated EEF. The difference depends on a radius and it is larger than 5 % at a radius smaller than 2 arcmin. The ratio plotted in Fig. 12(b) represents the systematic error of the effective area as a function of extraction radius. When extracting the spectrum within a radius smaller than 2 arcmin, the raytracing code xrtraytrace and thus the arf generator give ~5 % smaller effective area than that expected from the Crab EEF using the current mirror and detector calibrations. Therefore large extraction radius is recommended to avoid large systematic error of effective area and consequently the source flux estimation.

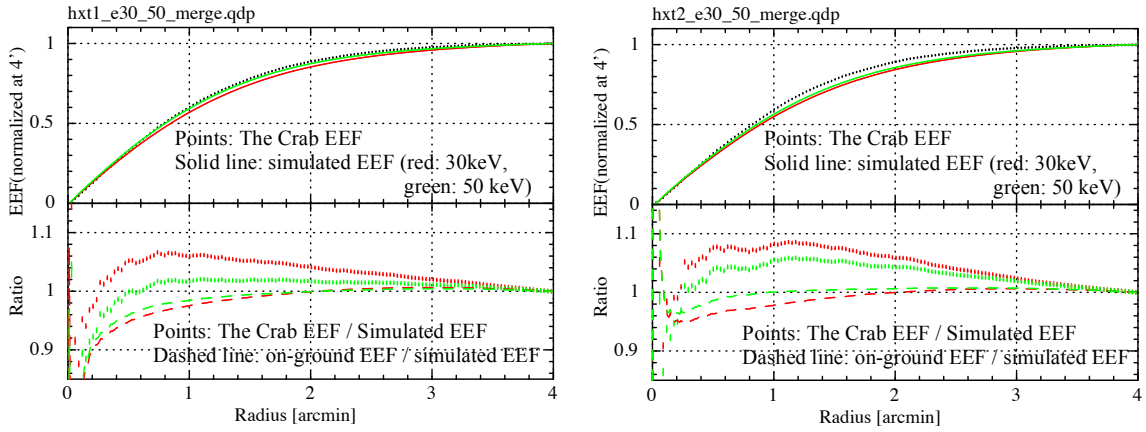

Fig. 12b Encircled Energy Function normalized at 4 arcmin (Upper panel, black points : the Crab pulsar in 8-80 keV, red solid line : simulated EEF at 30 keV, green solid line: simulated EEF at 50 keV) and ratio of observed to simulated EEF (bottom, red points: the Crab pulsar in 5-80 keV / simulated at 30 keV, green points: the Crab pulsar in 5-80 keV / simulated at 50 keV, red dashed line: on-ground EEF at 30 keV / simulated EEF at 30 keV, green dashed line: on-ground EEF at 50 keV / simulated EEF at 50 keV) .

Vignetting Function of each segment at 50 keV

Because vignetting function was measured at 50 keV in two orthogonal directions (θy and θz; see) for each segment independently, the vignetting function for the full telescope configuration has not been measured in any direction. In Fig. 13 and Fig. 14, the simulated vignetting functions of HXT1 and HXT2 were compared with measured ones by segment in two measured directions, respectively. Measured and simulated vignetting functions show in these figures are normalized by the peak effective area and its peak is aligned to offaxis angle = 0 arcmin. When offaxis angle < 2', simulated vignetting function is in quite good agreement with measured one as the difference is less than 5 %. Even for offaxis angle > 2', discrepancy is expected to be smaller than 10 %.

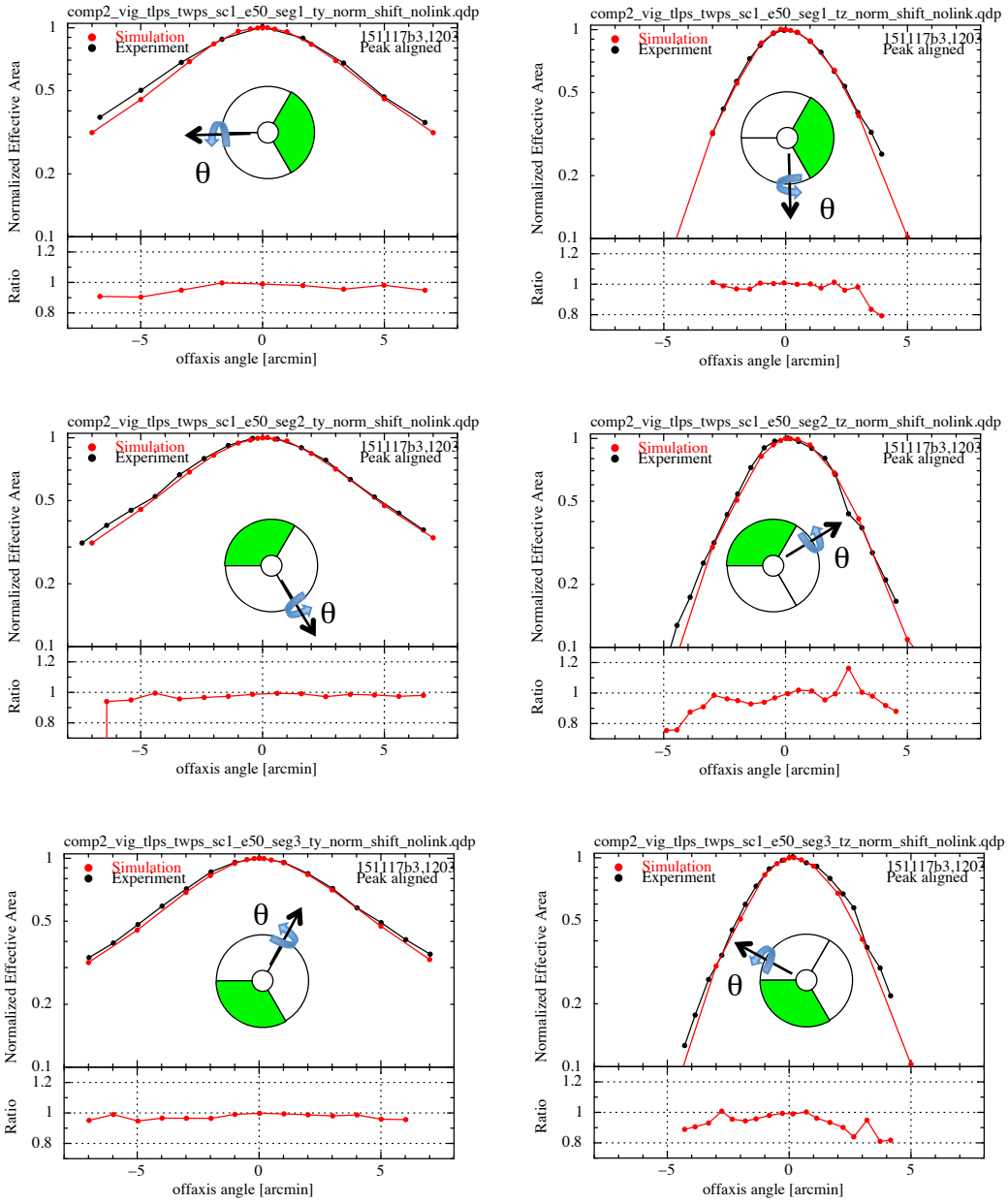

Fig. 13 Vignetting function of the segment 1 (top), the segment 2 (middle), segment 3 (bottom) of HXT-1 in θy (left) and θz (right) directions at 50 keV (segment number defined in the telescope definition file). Segment and rotation axis are shown in the inset figure.

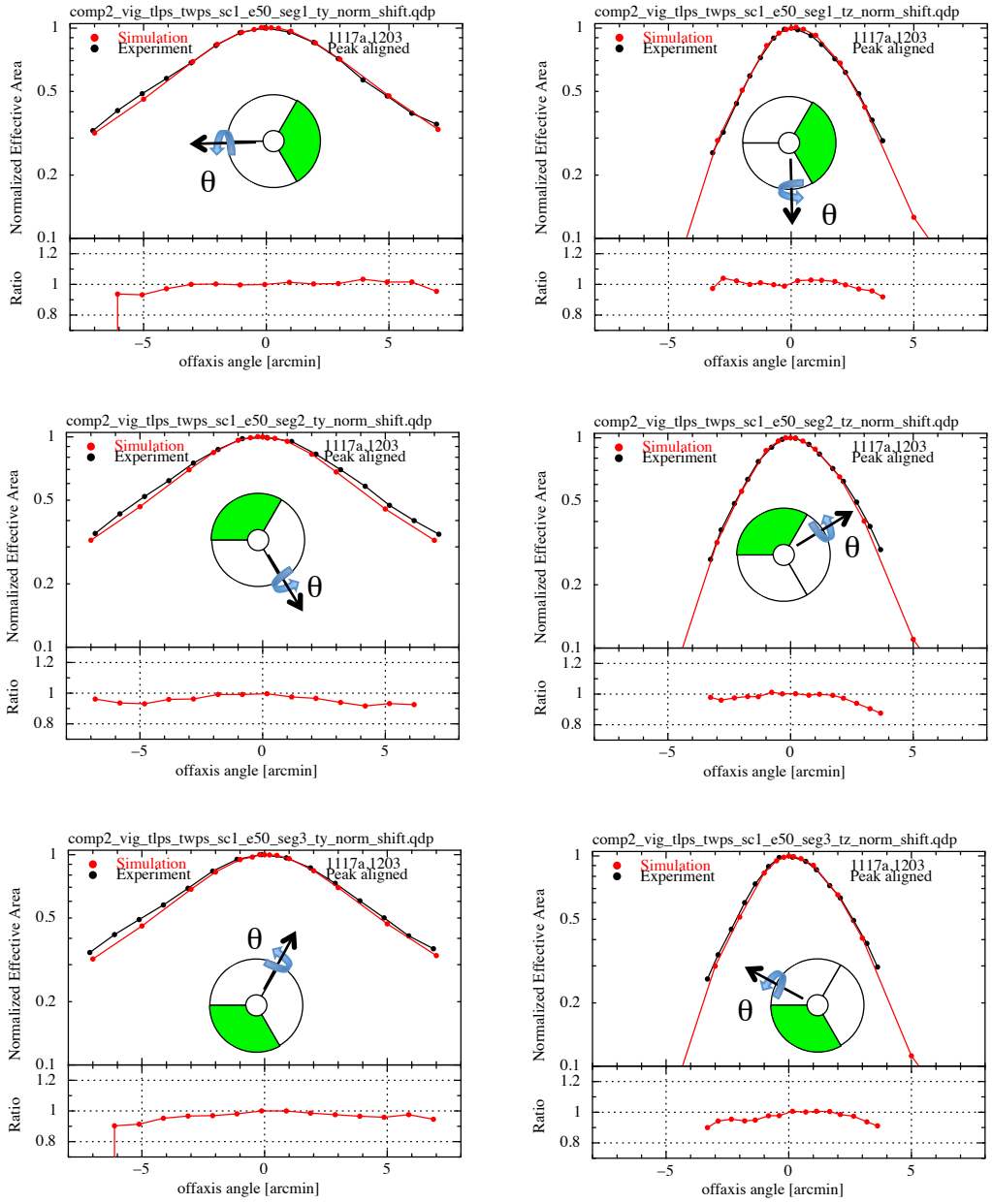

Fig. 14 Vignetting function of the segment 1 (top), the segment 2 (middle), segment 3 (bottom) of HXT-2 in θy (left) and θz (right) directions at 50 keV (segment number defined in the telescope definition file). Segment and rotation axis are shown in the inset figure.

Analytic function of Vignetting

For convenience to calculate ARF, analytic function representing the azimuthally averaged vignetting function of HXTs were obtained. Azimuthally averaged vignetting function was derived from simulated 2 dimensional vignetting maps at energies of 10 to 70 keV with 10 keV pitch with xrtraytrace and the current CALDB files, and fitted with the formula of lorentizan + constant;

$$f(E,\theta) = LN(E)\left(\frac{1}{1+\left(\frac{2\theta}{LW(E)}\right)^2} - 1\right) + 1$$

Here. E and θ are a energy in keV and an off axis angle in arcmin. The coefficients *LN(E)* and *LW(E)* are the functions of energy as followings,

For HXT1,

$$LW(E) = 14.865 - 5.323\exp(E/96.094)$$
$$LN(E) = -3.064 \times 10^{-4}E + 0.96278$$

For HXT2,

$$LW(E) = 10.224 - 1.148\exp(E/39.155)$$
$$LN(E) = -1.955 \times 10^{-4}E + 0.95755$$

Discrepancy between analytic function and simulated one are +/-5 % at E < 60 keV and +/-10 % at E ≥ 60 keV for HXT1, and +/- 5 % for HXT2 as shown in Fig. 15.
We should note that the difference shown here is not between measured data and the function but also between the xrtraytrace result and the function, and the analytic function is only applicable within a off axis angle of 7 arcmin.

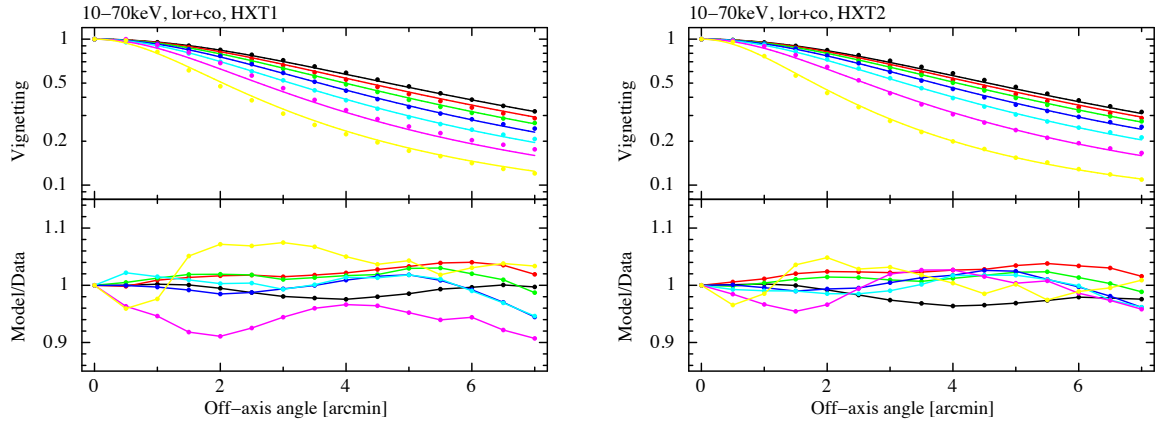

Fig. 15 Azimuthal averaged vignetting curve from the analytic function and raytracing simulation with xrtraytrace and the current CALDB files for HXT1 (left) and HXT2 (right). Bottom figures show the ratio of analytic function to xrtraytrace result. Dots and lines represent xrtraytrace and analytic function, respectively. Colors express different energies of 10 (black), 20 (red), 30 (green), 40 (blue), 50 (light blue), 60 (magenta) and 70 (yellow) keV.

2.4 Final remarks

The accuracy of simulation with the current CALDB files is estimated from the comparison with the ground calibration data taken at SPring-8; discrepancy of on-axis effective area between the simulation and the measurement is +/-9 % at energies of 8, 20, 30, 40, 50, 60 and70 keV, that of the EEF is 5 % or less at a radius larger than 2 arcmin, that of PSF is less than 20 % within a radius of 4 arcmin and at a radius > 4 arcmin, simulated PSF is 20 - 40 % fainter than the measured one.

3 Release CALDB 20161122

Filename	Valid data	Release date	CALDB Vrs	Comments
ah_hx1_mirror_20140101v001.fits	2014-01-01	20161122	005	Mirror
ah_hx2_mirror_20140101v001.fits	2014-01-01	20161122	005	Mirror
ah_hx1_reftrans_20140101v001.fits	2014-01-01	20161122	005	Reftrans
ah_hx2_reftrans_20140101v001.fits	2014-01-01	20161122	005	Reftrans
ah_hx1_auxtran_20140101v001.fits	2014-01-01	20161122	005	Fudge factor
ah_hx2_auxtran_20140101v001.fits	2014-01-01	20161122	005	Fudge factor

New mirror definition files are released for HXT-1 and HXT-2 but the only change was the addition of a new keyword (TELFPROT) that enables the updated xrtraytrace code to apply a rotation to the PSF with respect to the focal plane in order to match the output of the raytracing to the physical coordinate systems. Also released are new reflectivity files for HXT-1 and HXT-2. The only change in these files is the addition of data at several new energies to improve the energy grid. The final two files in the above table are new and (optionally) implement "fudge factors" to modify the effective area in the ARF and spectral response (RSP) files generated by aharfgen and hxirspeffimg. The data in these files is described below.

3.1 Data description

The "auxiliary transmission" factors (or fudge factors) that are used to modify the effective area generated by aharfgen and hxirspeffimg for HXI1 and HXI2 are adjustments to the effective area that are intended to account for the difference between the ground-based telescope effective area measurements and the telescope effective areas generated by the raytracing code xrtraytrace. The effective area produced by the raytracing code is controlled by the data in the mirror definition files, the reflectivity files, and the scattering files. Although the data in these files were fine-tuned to reproduce the ground-based effective areas as closely as possible by adjusting physical parameters relating to the physical properties of the telescopes, residuals of up to ~7% between the ground-based measurements and the raytracing predictions remained. These residual discrepancies have not been resolved in terms of identifying their physical origin. The CALDB files described here can be used optionally with aharfgen and hxirspeffimg to include the correction to the effective area in the ARF. Since the discrepancies are not negligible in the cases

of observing bright sources such as the Crab, the fudge factors are introduced to reproduce the effective area obtained from the on-ground calibration.

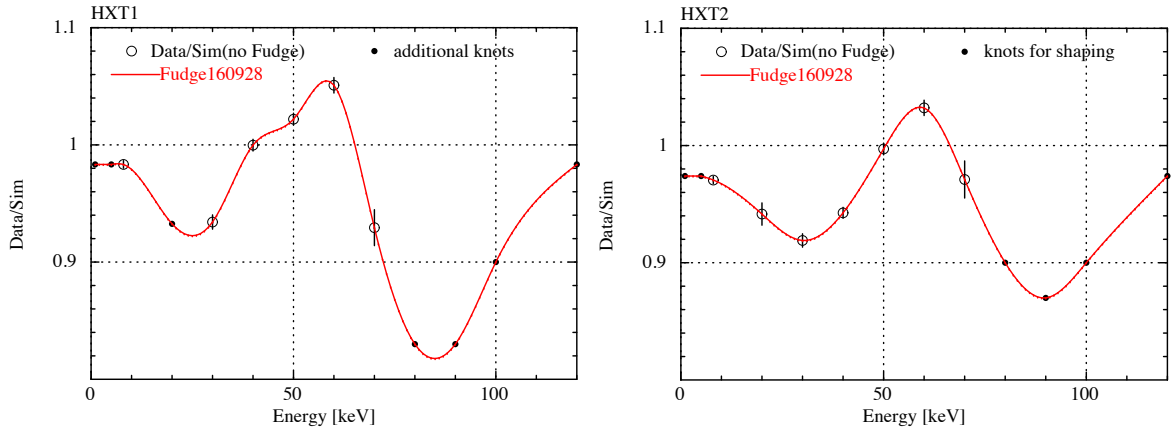

Fig. 16 Fudge factor as a function of energies (red solid line). Open circles with an error bar represent a ratio of effective area measured on the ground to that of the raytracing output with no fudge factor. Filled circles are additional knots to make the function smoothly converge with the raytracing output at the lowest and highest energy.

Fudge factor is a spline function which smoothly connects the ratios of measured to simulated effective area at 8, 30, 40, 50, 60 and 70 keV (and 20 keV only for HXT2) and additional knots to make the function converge with the raytracing output at the lowest and highest emergy as shown in Fig. 16.

3.2 Data analysis

Tools locally developed by the HXT team have been used to analyze the ground calibration data and estimate effective areas. To generate fudge factor table by spline interpolation, a perl script "*mk_arf_fudge160928.pl*" locally developed has been used.

3.3 Final remarks

The fudge factors introduced to reduce a discrepancy between the effective area measured on the ground and that of raytracing output.